

Illumination method for high resolution imaging at water surface

KOYO WATANABE

Unit of Measurement Technology, CEMIS-OULU, University of Oulu,
PO Box 51, 87101 Kajaani, Finland; e-mail: kouyouwatanabe@gmail.com

Annularly distributed light is proposed to increase the spatial resolution when observing a water surface. When light with an annular distribution is used to illuminate the entrance pupil of an objective lens, an air–water interface can be illuminated with a Bessel beam, which is a focused beam formed by plane wave components at the same angle. If the optimum size and width of the annular light and radial polarization are chosen, a microscopic distribution is obtainable from the reflected light intensity. It is theoretically shown that the reflectance changes with the width of annular light and this allows to make water surface measurements. In order to clarify the spatial resolution, the electric field intensity distribution on the focusing plane is also calculated. From the full width at half maximum of the calculated distribution, it is shown that the annularly distributed light increases the spatial resolution by increasing the radius of the annular light and decreasing the wavelength of the light. It is also shown that a spatial resolution of a few hundred nanometers is achievable.

Keywords: optical measurement, optical instrumentation, optical imaging.

1. Introduction

Instrumentation technology for detecting layers, molecules and particles at water interfaces has been a major concern in basic biophysical and biochemical research because the distribution and behavior of molecules are strongly related to studies of functionality of protein molecules [1, 2]. For example, the boundary region of micron or submicron structures of lipid bilayers [3], which serve as an ideal environment for analyzing the interactions of protein molecules, influences the behavior of protein molecules. In order to observe the micron and submicron patterns of molecules, it is necessary to use instrumentation technology with high sensitivity and high spatial resolution.

As one of the well-known instruments for molecular analysis on water surface, the fluorescence microscope is used to observe the distribution of molecules [4–6]. The measurement principle is that fluorescent molecules are used as a sensing probe and a region labeled with fluorescent molecules emits a signal of fluorescent light when the probe molecules are illuminated with excitation light. However, undesired

features are that this is an indirect observation and the fluorescent molecules have a detrimental influence on the behavior of observed objects [7]. Imaging of non-labeled molecules and direct observation clearly show the more specific behavior of molecules.

The use of infrared reflection absorption spectroscopy (IRRAS) was proposed to study the orientation and conformation of molecules on the water surface. In this method, a sample is illuminated with polarized infrared light at an optimal incident angle. By incorporating a polarization modulation (PM) system into the IRRAS, high-quality monolayer spectra can be detected [8]. Although this method exhibits good potential for water surface measurement, the spatial resolution of PM-IRRAS is only $\sim 12 \mu\text{m}$ [9] because it is dependent on the numerical aperture of the objective lens and the wavelength of the infrared light. This low resolution limits the observation of micron and submicron patterns of molecules.

Brewster angle measurement is also a well-known method for analyzing a water surface [10–12]. The setup typically consists of a source of light and a CCD device looking through a lens, and the laser illuminates the interface of two different dielectric media. The relationship between reflectance and incident angle is given by the Fresnel equations. When two different dielectric media and *p*-polarized light are assumed, there is an angle at which light is perfectly transmitted through the interface with no reflection. This phenomenon has been used as a method for interfacial analysis because reflected light appears if there exists an interfacial layer with roughness; this is because the refractive index changes at the interface. The sensitivity based on this is high enough to detect particles and a monolayer of molecules. The advantages of these sensors are that nondestructive measurements are possible, with high sensitivity, high speed, and wide area of observation.

Ellipsometry is another type of reflectometry where the reflected light is measured as a signal [13–15]. The advantages of these methods are that measurements of polarization changes are possible, nondestructively, with high sensitivity, high speed, and wide of area observation. They allow direct and non-label observations and detect the optical properties of the sample. A commercial sensor basically consists of a source of light and a photodiode looking through a set of filters. With an appropriate incident angle and polarization, the light illuminating the interface is reflected and the reflected light is detected as a signal. The sensing region of both sensors is basically determined by the illuminated region of laser light. In these sensors, the minimum size of the illuminated region is normally $\sim 2 \mu\text{m}$ [16].

In achieving a small illuminated region with a size of a few hundred nanometers, the value of these sensors is increased dramatically; one can use it to analyze a nanostructured sample located at a water interface and the illumination power of the light source can be efficiently used by condensing the rays of light. A focused laser beam is a method of making an illuminated region which is optically diffraction-limited. However, it is difficult to utilize this to focus the laser beam for the above purposes for two reasons: *i*) a focused laser beam is composed of plane waves having different

incident angles; *ii)* the direction of polarization changes when the plane wave of the illuminating light passes through the objective lens because of refracted rays.

In this paper, to achieve focused beam illumination with an appropriate incident angle and polarization, an illumination system using annularly distributed light is proposed. An objective lens converts the distribution to a zeroth-order Bessel beam [17], which is a focused beam formed by plane wave components at the same angle. Under illumination, a method to control the incident angle and polarization is also shown. With the proposed illumination system, in order to clarify the spatial resolution, the electric field intensity distribution of the illumination light in the air space on the focusing plane is calculated and it is shown that the proposed illumination system increases the spatial resolution.

2. Calculation model

Figure 1 shows the proposed illumination system used to illuminate with a focused laser beam composed of plane waves with the same incident angle α . In the system, annularly distributed light is directed at the entrance pupil plane of an objective lens. Then the objective lens converts the annular distribution to a Bessel beam, which is formed by plane wave components with the same incident angle. The focusing angle α can be changed by controlling the radius of the annularly distributed light. The angle α can be expressed in terms of the numerical aperture (NA) of the objective lens:

$$\alpha = \arcsin\left(\frac{NA}{n_1}\right) \quad (1)$$

where n_1 denotes the refractive index of the incident dielectric medium. The radius can be changed by using a zoom lens and a telecentric system incorporated on the back side of the objective lens [18].

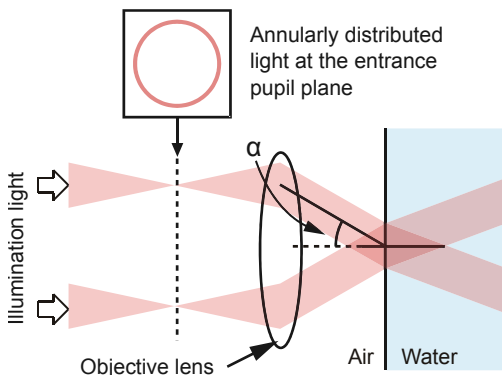


Fig. 1. A model of the annularly distributed light illumination on the entrance pupil plane of the objective lens. The air–water interface is illuminated with a focused laser beam at the same incident angle.

3. Results

3.1. Polarization dependence

Choosing *p*-polarized light is essential for obtaining good sensitivity because *s*-polarized light components do not contribute to the image formed in Brewster angle measurements; this is because *s*-polarized light components lack illumination power. In the case of focused beam illumination, a particular polarization is required. This is because most plane wave components are divided into *p*- and *s*-polarization when the wave passes through the objective lens because of refracted rays. To utilize the incident light intensity efficiently, and to illuminate with *p*-polarized light from all directions, radially polarized light is required [19, 20].

To show the efficacy of radial polarization in interfacial measurements and in the proposed illumination system, the reflectance is calculated. The calculation method has been described in [21]. In the calculation, it is assumed that the entrance pupil is illuminated with light with an annular distribution and with linear and radial polarizations. The width of the annularly distributed light is assumed to be 0.02. The radius of the annular light is adjusted to a numerical aperture of 0.79–0.81. An aperture of 0.80 corresponds to a Brewster angle $\theta_B = \text{atan}(1.33)$. It is also assumed that the illuminating light is focused at the air (1.00)–water (1.33) interface. Figure 2a shows the oscillatory nature of the linearly polarized light at the entrance pupil.

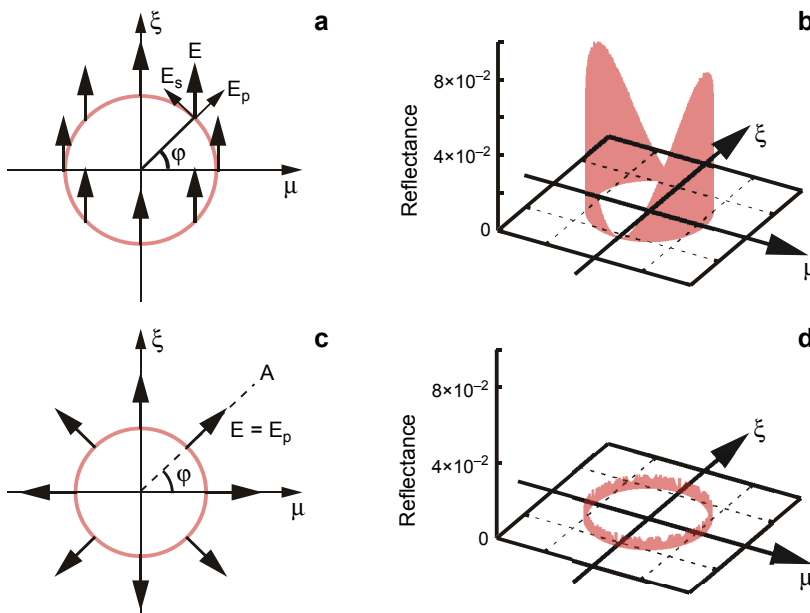


Fig. 2. The reflectance distribution on the exit pupil plane (b and d) using linearly (a) and radially (c) polarized light with an annular distribution, respectively.

The amplitude of the electric field E oscillating along the direction of ξ can be divided into p - and s -polarized components with φ . The components of p -polarized light E_p and s -polarized light E_s can be expressed as $E \sin \varphi$ and $E \cos \varphi$. The light passing at angles of $\varphi = 90^\circ$ and 270° , and 0° and 180° , is completely p -polarized light and s -polarized light, respectively. Figure 2**b** shows the result of the calculation of reflectance at the exit pupil. At angles corresponding to 90° and 270° , one can see that the reflectance is reduced compared to the other illuminated regions. Figure 2**c** shows the oscillating directions of radially polarized light at the entrance pupil. The amplitude of the electric field E corresponds to E_p . Figure 2**d** shows the calculated result. The reflectance calculated at the exit pupil plane is 2.0×10^3 times smaller than that for linearly polarized light. It is evident that by using radially polarized light, the illumination power can be efficiently used for Brewster angle measurements, and therefore, the use of radially polarized light is optimal for the proposed illumination system.

The reflectance depends not only on the polarization but also on the range of incident angles. In the illumination system, the range is determined by the width and radius of the annularly distributed light at the entrance pupil. The range $\delta\theta_i = \theta_{\text{outer}} - \theta_{\text{inner}}$ can be expressed in terms of the numerical aperture (NA) of the objective lens:

$$\delta\theta_i = \arcsin\left(\frac{\text{NA}_{\text{outer}}}{n_1}\right) - \arcsin\left(\frac{\text{NA}_{\text{inner}}}{n_1}\right) \quad (2)$$

where NA_{inner} and NA_{outer} denote the inner and outer parts of the annularly distributed light, respectively. Here, the reflectance R_p is expressed as a function of the incident angle, based on the Fresnel equation:

$$R_p = \frac{1}{A} \int_{\theta_{\text{inner}}}^{\theta_{\text{outer}}} \left| \frac{\tan \left[x - \arcsin \left(\frac{n_1}{n_2} \sin x \right) \right]}{\tan \left[x + \arcsin \left(\frac{n_1}{n_2} \sin x \right) \right]} \right|^2 dx \quad (3)$$

where x and A denote the angle and intensity of the incident light, respectively. Figure 3 shows the calculated reflectance as a function of the width of the annular light using Eqs. (2) and (3). In the calculation, a numerical aperture corresponding to the Brewster angle at the center of the width, and refractive indices n_1 and n_2 having values of 1.00 and 1.33 are assumed. The plot shows that the reflectance changes with the width of the annularly distributed light.

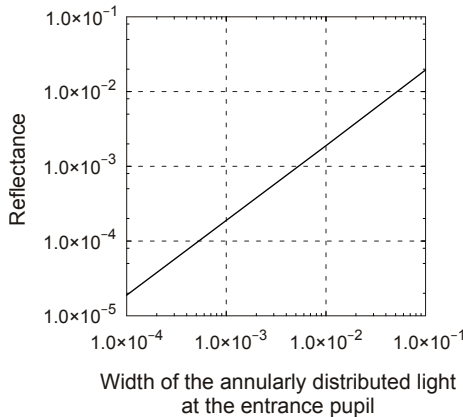


Fig. 3. Plot of the reflectance calculated as a function of the width of the annularly distributed light.

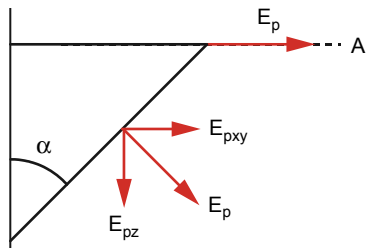


Fig. 4. The electric field E corresponding to the line A shown in Fig. 2c. Each of the components of E is shown.

From the calculated result, it can be theoretically estimated that the reflectance depends on the width of the annularly distributed light and a width of less than 1.0×10^{-5} is required to obtain sufficient sensitivity to observe monolayers because a reflectance of $\sim 1.0 \times 10^{-6}$ is necessary to detect a lipid monolayer.

3.2. Electric field intensity distribution

The extent of the electric field distribution of a focused laser beam determines the spatial resolution. The size of the distribution depends on the wave number of the illuminating light making up the focused beam: the focusing angle and wavelength of the illuminating light strongly affect the size. To show the positive effect of the proposed illumination system in increasing the spatial resolution, the electric field intensity distribution is calculated.

The electric field intensity ($It = |E_x|^2 + |E_y|^2 + |E_z|^2$) on the focusing plane can be calculated by superposing plane wave components of E_x , E_y , and E_z . Figure 4 indicates the electric field E corresponding to the line A shown in Fig. 2c and its components. In the case of radial polarization, the field E is composed of p -polarized components E_p since the field is oscillating in the incident plane. The electric field distribution of each of the components E_x , E_y , and E_z on the focusing plane can be expressed in terms of α , φ , and the phase as a function of position $\exp[-i(k_x x + k_y y + k_z z)]$:

$$E_x = E_p \cos(\alpha) \cos(\varphi) \exp[-i(k_x x + k_y y + k_z z)] \quad (4)$$

$$E_y = E_p \cos(\alpha) \sin(\varphi) \exp\left[-i(k_x x + k_y y + k_z z)\right] \quad (5)$$

$$E_z = E_p \sin(\alpha) \exp\left[-i(k_x x + k_y y + k_z z)\right] \quad (6)$$

Figure 5a shows the calculated electric field intensity It distribution in air space. In the calculation, as illuminating light, annularly distributed light and circularly distributed light on the entrance pupil plane are assumed, as shown in Figs. 5a and 5g. Radial polarization and a wavelength of 632.8 nm are assumed as the light source. Figures 5b–5d and 5h–5j show the electric field intensity for the E_x , E_y , and E_z components, respectively. The images of (e) and (k) show the electric field intensity

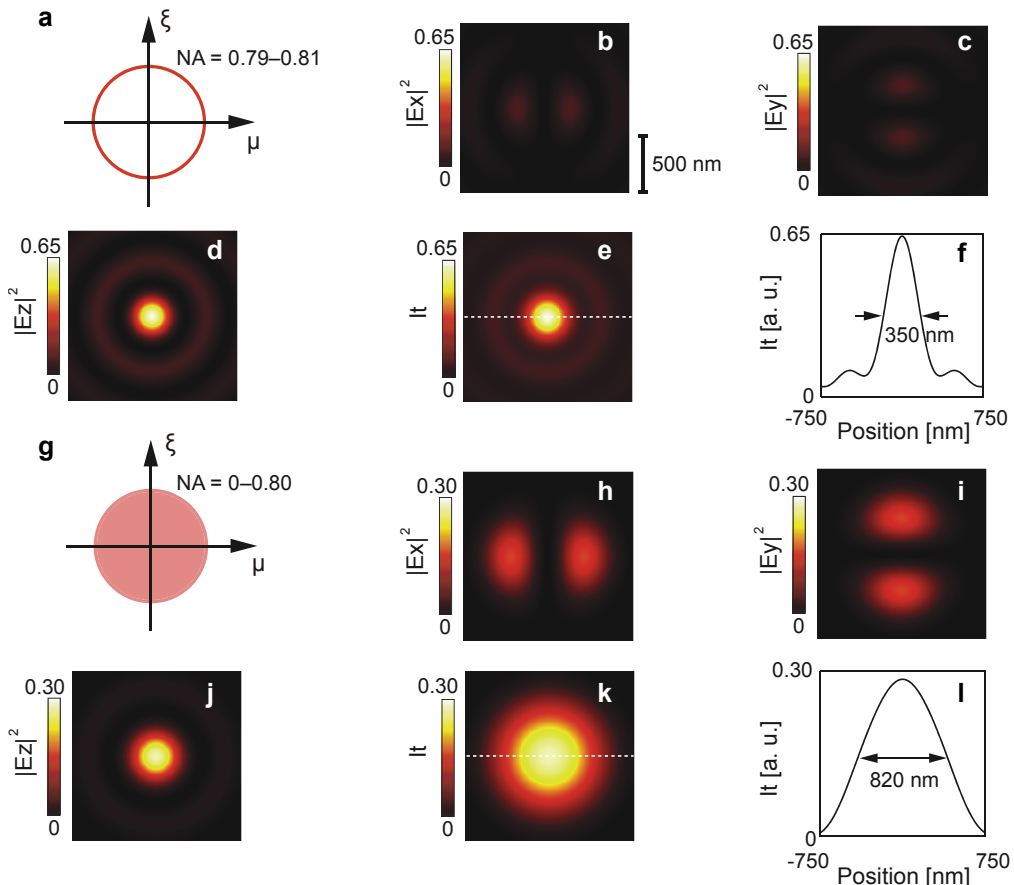


Fig. 5. Calculated electric field intensity distribution assuming radially polarized light for annularly distributed light and circularly distributed light illumination. Images (a) and (g) show the illuminated distribution on the entrance pupil plane. Images (b)–(d) and (h)–(j) are electric field intensity distributions for components E_x , E_y , and E_z , respectively. Images (e) and (k) are the intensity distribution It and plots (f) and (l) are the line profiles corresponding to the white dotted line on images (e) and (k), respectively. The calculated region shown in images (b)–(e) and (h)–(k) has an area of $1.5 \mu\text{m} \times 1.5 \mu\text{m}$.

It superimposed with $|E_x|^2$, $|E_y|^2$, and $|E_z|^2$. The plots of (f) and (l) are line profiles corresponding to the white dotted line on the images of (e) and (k). The full width at half maximum (FWHM) of the electric field intensity It for each illumination are 350 nm and 820 nm. From the calculated results, one can see that the annularly distributed light makes the 470 nm field smaller than with circular illumination. This is because of the difference of ratios between E_z and the other components E_x and E_y . The E_z components make a single peak distribution. On the other hand, the E_x and E_y components make two peaks about the optical axis and this increases the FWHM. In the case of annularly distributed light, the E_z components are dominant. However, the circularly distributed light covers center parts of the pupil plane, and the light passing through the center part of the pupil makes E_x and E_y the dominant fields. From these results, to obtain high spatial resolution, annularly distributed light with a sufficiently large radius should be used.

The electric field intensity It distribution is calculated as a function of the size of annularly distributed light. The width of the annularly distributed light and the wavelength of the light are assumed to be 0.02NA and 632.8 nm, respectively, in this calculation. Figure 6a shows the FWHM plots. One can see that the FWHM, which indicates the spatial resolution, decreases because of the increased extent of the annularly distributed light (e.g., when NA is assumed to be 0.8, which is the Brewster angle at the water-air interface, the FWHM is \sim 350 nm).

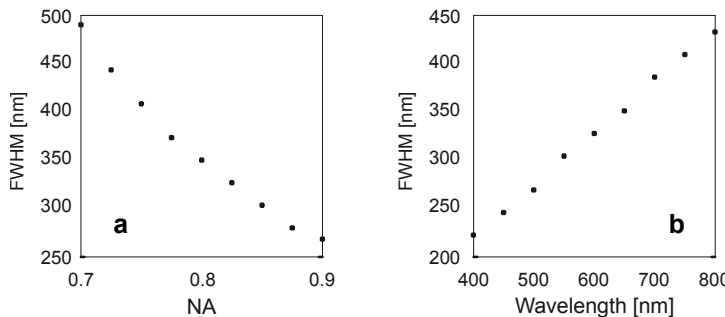


Fig. 6. FWHM plots of electric field intensity It distribution. FWHM plots as a function of NA (a), FWHM plots as a function of wavelength (b).

Because choosing the wavelength of the light also affects the spatial resolution, the FWHM is calculated as a function of wavelength. Figure 6b shows the FWHM curve as a function of wavelength. In the calculation, the extent of the annularly distributed light is assumed to be 0.8NA. The FWHM decreases with decreasing wavelength.

4. Conclusions

An illumination method using annularly distributed light has been proposed to increase the spatial resolution. It has been theoretically shown that annularly distributed light

with a radial polarization allows high spatial resolution imaging at air–water interfaces. It has been shown that the reflectance depends on the width of the annularly distributed light at the entrance pupil, and a spatial resolution of the order of a few hundred nanometers can be achieved by choosing a short wavelength of light and optimal size of annular light. For the practical verification of the proposed method, a set of an axicon and a Fourier transform lens can possibly be used as an optical system to generate annularly distributed light and carry out high-resolution imaging of objects at air–water interface.

Acknowledgements – This work has been supported in part by the Joint authority of Kainuu Region, the Fuji Foundation for Protein Research, and the Scandinavia–Japan Sasakawa Foundation.

References

- [1] MONTANHA E.A., PAVINATTO F.J., CASELI L., KACZMAREK O., LIEBSCHER J., HUSTER D., OLIVEIRA O.N. JR., *Properties of lipophilic nucleoside monolayers at the air–water interface*, Colloids and Surfaces B: Biointerfaces **77**(2), 2010, pp. 161–165.
- [2] LE FLOCHE-FOUÉRÉ C., BEAUFILS S., LECHEVALIER V., NAU F., PÉZOLET M., RENAULT A., PEZENNÉC S., *Sequential adsorption of egg-white proteins at the air–water interface suggests a stratified organization of the interfacial film*, Food Hydrocolloids **24**(4), 2010, pp. 275–284.
- [3] LIN W.-C., BLANCHETTE C.D., RATTO T.V., LONGO M.L., *Lipid asymmetry in DLPC/DSPC-supported lipid bilayers: A combined AFM and fluorescence microscopy study*, Biophysical Journal **90**(1), 2006, pp. 228–237.
- [4] LÖSCHE M., SACKMANN E., MÖHWALD H., *A fluorescence microscopic study concerning the phase diagram of phospholipids*, Berichte der Bunsen-Gesellschaft für Physikalische Chemie **87**(10), 1983, pp. 848–852.
- [5] WEIS R.M., McCONNELL H.M., *Two-dimensional chiral crystals of phospholipid*, Nature **310**, 1984, pp. 47–49.
- [6] MOORE B., KNOBLER C.M., BROSETA D., RONDELEZ F., *Studies of phase transitions in Langmuir monolayers by fluorescence microscopy*, Journal of the Chemical Society Faraday Transactions 2: Molecular and Chemical Physics **82**(10), 1986, pp. 1753–1761.
- [7] MEUNIER J., LANGEVIN D., BOCCARA N., *Physics of Amphiphilic Layers*, Springer Verlag, Berlin, 1987.
- [8] BLAUDEZ D., BUFFETEAU T., CORNUT J.C., BESBAT B., ESCAFRE N., PÉZOLET M., TURLET J.M., *Polarization-modulated FT-IR spectroscopy of a spread monolayer at the air/water interface*, Applied Spectroscopy **47**(7), 1993, pp. 869–874.
- [9] STEINER G., SABLINSKAS V., SEIDEL W., SALZER R., *PM-IRRAS mapping of ultrathin molecular films with high spatial resolution*, Analytical and Bioanalytical Chemistry **395**(6), 2009, pp. 1641–1650.
- [10] KOZARAC Z., MÖBIUS D., MARTIN ROMERO M.T., *Characterization of aquatic natural microlayers by monolayer techniques and Brewster angle microscopy*, Water Research **34**(5), 2000, pp. 1463–1472.
- [11] LU SUN, MIAO XU, XUELIANG HOU, LIXIN WU, *In-situ observation of the aggregated morphology and interaction of dialkyldimethylammonium bromide with DNA at air/water interface by Brewster angle microscopy*, Materials Letters **58**(9), 2004, pp. 1466–1470.
- [12] MURRAY B.S., XU R., DICKINSON E., *Brewster angle microscopy of adsorbed protein films at air–water and oil–water interfaces after compression, expansion and heat processing*, Food Hydrocolloids **23**(4), 2009, pp. 1190–1197.
- [13] KEDDIE J.L., *Structural analysis of organic interfacial layers by ellipsometry*, Current Opinion in Colloid and Interface Science **6**(2), 2001, pp. 102–110.

- [14] WONGMANEROD C., ZANGOOIE S., ARWIN H., *Determination of pore size distribution and surface area of thin porous silicon layers by spectroscopic ellipsometry*, Applied Surface Science **172**(1–2), 2001, pp. 117–125.
- [15] BELLET-AMALRIC E., BLAUDEZ D., DESBAT B., GRANER F., GAUTHIER F., RENAULT A., *Interaction of the third helix of Antennapedia homeodomain and a phospholipid monolayer, studied by ellipsometry and PM-IRRAS at the air–water interface*, Biochimica et Biophysica Acta (BBA) – Biomembranes **1467**(1), 2000, pp. 131–143.
- [16] NASIR M.N., THAWANI A., KOUZAYHA A., BESSON F., *Interactions of the natural antimicrobial mycosubtilin with phospholipid membrane models*, Colloids and Surfaces B: Biointerfaces **78**(1), 2010, pp. 17–23.
- [17] DURNIN J., *Exact solutions for nondiffracting beams. I. The scalar theory*, Journal of the Optical Society of America A **4**(4), 1987, pp. 651–654.
- [18] WATANABE K., TERAKADO G., KANO H., *Localized surface plasmon microscope with an illumination system employing a radially polarized zeroth-order Bessel beam*, Optics Letters **34**(8), 2009, pp. 1180–1182.
- [19] WATANABE K., HORIGUCHI N., KANO H., *Optimized measurement probe of the localized surface plasmon microscope by using radially polarized illumination*, Applied Optics **46**(22), 2007, pp. 4985–4990.
- [20] MIYAJI G., OHBAYASHI K., SUEDA K., TSUBAKIMOTO K., MIYANAGA N., *Generation of vector beams with axially-symmetric polarization*, The Review of Laser Engineering **32**(4), 2004, pp. 259–264.
- [21] KANO H., KNOLL W., *Locally excited surface-plasmon-polaritons for thickness measurement of LBK films*, Optics Communications **153**(4–6), 1998, pp. 235–239.

Received May 10, 2010
in revised form September 16, 2010